Weather and Climate Extremes xx (xxxx) xxxx–xxxx

Contents lists available at ScienceDirect

Weather and Climate Extremes

journal homepage: www.elsevier.com/locate/wace

A new flood type classification method for use in climate change impact studies

Thea Turkington[a,*], Korbinian Breinl[b], Janneke Ettema[a], Dinand Alkema[a], Victor Jetten[a]

[a] Faculty of Geo-Information Science and Earth Observation (ITC), University of Twente, Enschede, The Netherlands
[b] Department of Geoinformatics, Paris-Lodron University of Salzburg, Salzburg, Austria

A B S T R A C T

Flood type classification is an optimal tool to cluster floods with similar meteorological triggering conditions. Under climate change these flood types may change differently as well as new flood types develop. This paper presents a new methodology to classify flood types, particularly for use in climate change impact studies. A weather generator is coupled with a conceptual rainfall-runoff model to create long synthetic records of discharge to efficiently build an inventory with high number of flood events. Significant discharge days are classified into causal types using k-means clustering of temperature and precipitation indicators capturing differences in rainfall amount, antecedent rainfall and snow-cover and day of year. From climate projections of bias-corrected temperature and precipitation, future discharge and associated change in flood types are assessed. The approach is applied to two different Alpine catchments: the Ubaye region, a small catchment in France, dominated by rain-on-snow flood events during spring, and the larger Salzach catchment in Austria, affected more by rainfall summer/autumn flood events. The results show that the approach is able to reproduce the observed flood types in both catchments. Under future climate scenarios, the methodology identifies changes in the distribution of flood types and characteristics of the flood types in both study areas. The developed methodology has potential to be used flood impact assessment and disaster risk management as future changes in flood types will have implications for both the local social and ecological systems in the future.

1. Introduction

Climate change will alter flooding around the globe, and therefore an increasing number of studies are modelling the impact of climate change on floods, with the focus generally on changing magnitude and frequency of the flood events (Booij, 2005; Gain et al., 2013; Raff et al., 2009). However, future projections of the meteorological triggers, including heavy precipitation and snowmelt, may change differently and alter the characteristics of the flood events (Hall et al., 2014). As a result, factors associated with the causal type of flood such as seasonality and triggering conditions should be addressed next to the change in frequency or magnitude of floods. Classifying flood events into different types can place flooding into a wider climate context and help with exploring changes in future flood events. Changes in flood types will have implications on both the local social and ecological systems and are therefore important to consider when assessing future changes in flooding (Gain et al., 2013; Garner et al., 2015).

Flood types can be distinguished based on the meteorological conditions of a flood event, such as amount and distribution of precipitation, as well as antecedent conditions, such as snow depth and soil moisture. Nied et al. (2014) identify three different approaches to describe flood events: (1) based on the flood event description, (2) linking the flood with atmospheric circulation patterns, and (3) classification into flood types. The first category describing the specific flood events covers studies with a detailed examination of a particular event (e.g. the Danube flood in 2013 (Blöschl et al., 2013), the Mississippi River flood in 1993 (Kunkel et al., 1994), and the Himalayan flood in 2013 (Dube et al., 2014)). The second approach uses large scale atmospheric circulation patterns to identify similar atmospheric triggering conditions that are linked with the probability of flood occurrence (e.g. Bárdossy and Filiz, 2005; Delgado et al., 2014; Pattison and Lane, 2012; Prudhomme and Genevier, 2011). In the final approach, individual flood events are clustered into different categories based on generating processes of the events (e.g. Gaál et al., 2012; Merz and Blöschl, 2008; Viglione et al., 2010).

Of the three approaches for identifying flood types, the applicability of the method depends on the purpose. The description of flood events allows for a singular flood event to be examined, without necessarily a long record of events. However, the variables considered vary between case studies, in part due to different data availability, making it difficult

* Corresponding author.
E-mail address: turkington29881@alumni.itc.nl (T. Turkington).

http://dx.doi.org/10.1016/j.wace.2016.10.001
Received 18 November 2015; Received in revised form 30 September 2016; Accepted 4 October 2016
Available online xxxx

to compare between case studies (Nied et al., 2014). Widely applied classification based on atmospheric conditions is hampered due to the small number of actual flood events relative to the overall number of days (Nied et al., 2014; Prudhomme and Genevier, 2011), particularly on the local or regional scale where maybe only a handful of observed flood events occurred over the past 100 years. Both the second and third categories have the potential to be used in climate change impact studies, provided there are sufficient flood events, and that climate models are able to reproduce the necessary atmospheric variables. Even with long complete records, a relationship between flood events and large scale atmospheric circulations cannot be determined in many cases. Therefore, the classification approach (approach three) will be applied here, as the characteristics of the flood events are of concern in assessing the impact of climate change on flood types.

The variety of approaches to cluster flood events leads to different flood types. The approach to cluster flood events depends on the region and triggering conditions as well as the data available. Merz and Bloschl (2003) clustered flood types manually allowing a combination of different sources of information to be used. They classified the flood events into five types: flash floods, short rain, long rain, rain-on-snow, and snowmelt floods. Nied et al. (2014) used the previous classification of five flood types, and then compared the soil moisture and atmospheric circulation patterns between flood types, highlighting the importance of antecedent conditions for the different flood types. Alila and Mtiraoui (2002) clustered flood events based on ENSO, storms (monsoonal storms, frontal storms and dissipating tropical cyclones), with either two or three clusters for each classification for south-east and central Arizona in the USA. Viglione et al. (2010) included catchment excess rainfall as part of the flood response for different flood types in the Kamp catchment, Austria, while Gaál et al. (2012) clustered different Austrian catchments including the month when it occurred. In each of these studies, to obtain sufficient number of flood events, either less severe flood events were included or a large study area was defined, incorporating discharge measurements from multiple locations a catchment or catchments. Therefore, we introduce the use of a weather generator in combination with conceptual rainfall-runoff model to generate long time series of discharge to classify flood types.

Little research has been done on how causal flood types explicitly will change in the future and recent literature provides evidence that they will change along with potential indicators to use in classifications. Arnell and Gosling (2014) found decreases in magnitude of spring floods for central Europe as a result of smaller discharge peaks from rainfall than the previously snowmelt-generated ones. Possible future changes in flood seasonality have also been identified in Switzerland due to changes in rainfall, snow accumulation, and snow melt (Köplin et al., 2014). Current trends in rain-on-snow floods in the western United States have a range of significant increasing and decreasing trends (McCabe et al., 2007). In the future, parts of the same area are expected to shift from snow dominated winters to rain dominated winters (Nolin and Daly, 2006). An increase of high temperature and heavy rainfall in Norway also indicates an increase in winter/spring snowmelt floods (Benestad and Haugen, 2007; Vormoor et al., 2015). While none of these studies considered changing flood types explicitly, they demonstrate that changes in precipitation, both rainfall and snowfall and melt have the potential to alter flood types in a catchment.

This paper presents a methodology developed to classify flood types particularly for use in climate change impact studies as it creates and analyzes long records (meteorological and flood events). To obtain sufficiently long records of flood events for objective flood type classification, a multi-site weather generator is coupled with the HBV rainfall-runoff model. The flood events are extracted from the resulting 1200 years of simulated data, where a flood is defined as days with discharge that could potentially lead to flood situations. In particular the discharge levels corresponded to the 2 (bank full flow), 10, and 25 year return periods, with longer return periods were not considered in order to limit spurious extrapolations. The flood events are separated into different flood types based on extreme meteorological triggering conditions and flood timing (Section 2). To illustrate the developed methodology, two European catchments are used as test sites with different sizes and dominant flood types (Sections 3 and 4). In this paper we apply the methodology to future climate projections and on the past climate (Section 5), allowing new flood types to be identified that were absent in the past. Four different climate projections are analyzed for each catchment for the period 2070–2099 to demonstrate how changes in the future climate may alter flood types in the future. Sections 6 and 7 discuss and conclude our findings.

2. Methods

In any classification method, a sufficient number of events is required to allow for clustering. In the case of flood events within a single catchment there are often only a handful of events. While other studies work around this through the using multiple catchments, this paper aims to classify the flood types within a catchment by producing synthetic data based on observational records. Long time series of meteorological and hydrological data is generated using a combination of a weather generator (Section 2.1) and model of discharge (Section 2.2). Once this synthetic time series is generated for past and future climate, clustering of different flood types can be done (Section 2.3). A flow diagram of all steps of the methodology is contained in the Supplementary material.

2.1. Weather generator

The semi-parametric daily-multisite weather generator from Breinl et al. (2014) was utilized to generate long time series of daily 2 m temperature and precipitation values to serve as input for the rainfall-runoff model. The multi-site precipitation algorithm uses a univariate Markov process to represent sequences of daily snapshot of precipitation amounts for multiple point locations within the catchment. The weather generator was used in a so-called Reduced State Space setup (see Breinl (2015) and Breinl et al. (2014)) to reduce the duplication of observed precipitation sequences. Precipitation amounts were simulated by pure resampling of observations ('bootstrap'), instead of using parametric distribution functions for precipitation amounts as applied in Breinl et al. (2014). Parametric distributions were not applied to do the complexity of altering compound distributions under future climate scenarios. For the temperature, mean daily temperature was simulated with autoregressive-moving-average processes (ARMA). The weather generator was set up monthly to account for seasonality of precipitation and temperature. In total 1200 years of daily temperature and precipitation were generated to drive the conceptual rainfall-runoff model (see Section 2.2) for the observed period, as well as for each of the selected future climate projections.

The multi-site weather generator has been successfully applied for the historical period in Alpine catchments by Breinl (2015). It was found that the weather generator handles the spatial variability of precipitation between rain gauges well, with a slight tendency to underestimate extreme dry spells, which is a well-known issue of Markov based weather generation algorithms. The mean number of dry and wet days was well simulated.

To generate future projections of precipitation, the time series of the resampled observational period values were first generated by the weather generator and then the values replaced with the projected precipitation amounts by reshuffling to maintain temporal and inter-site statistics. Future temperature projections were generated by adding the projected monthly mean temperature shift to the observations, a common technique in climate impact studies (e.g. Steinschneider and Brown, 2013; Tao and Zhang, 2011). These generated time series are fed to the HBV model to simulate future discharge.

2.2. HBV model

The conceptual HBV rainfall-runoff model was used to model historical and future discharge based on observational records and future climate data (Bergström, 1976). The HBV model was selected as it represents the main runoff generating processes, and due to the low computational costs, it can be used to generate discharge time series longer than 1000 years. The model has also been used in numerous previous studies (e.g. Booij, 2005; Das et al., 2008; Gao et al., 2012; Steele-Dunne et al., 2008). For this study, the HBV-light model (version 4.0.0.6) from Seibert and Vis (2012) was applied. The model was used in a semi-distributed setup, with a single catchment sliced into ten elevation zones for distributed snow modelling a well as three groundwater boxes. The HBV-light model uses time series of daily precipitation, daily mean temperature and daily discharge data for calibration. For historical period, multi-site precipitation from the weather generator in Section 2.1 was averaged through Thiessen polygons, which turned out to be sufficient compared to other methods such as Kriging with external drift (Breinl, 2015). The potential monthly evaporation was calculated after Thornthwaite (1948), as has been used in previous studies in combination with the HBV model (e.g. Bergström et al., 2001; Akhtar et al., 2008; Timalsina et al., 2015).

The HBV model was calibrated and validated based on 20 years of observed temperature, precipitation, and discharge as a 20 year period has been assessed to be sufficient length for use in climate change impact studies (Vaze et al., 2010). For the calibration, the ranges of 15 model parameters were taken from Seibert and Vis (2012), related to snow, soil moisture, response, and routing. In total 100 different parameter sets were calibrated to account for equifinality (Beven, 1999) using a genetic algorithm followed by Powell's quadratically convergent method for fine-tuning (Press et al., 2002). Further details on the calibration and validation process as well as the model performance in both catchments can be taken from Breinl (2015). After model calibration, synthetic discharge (1200 years) was generated by feeding the temperature and precipitation time series from the weather generator in Section 2.1 into the HBV model. This was done for both the past and future periods. As different magnitude flood events may have differences in flood type characteristics, three discharge magnitudes were used. These were based on the 2 (bank full), 10, and 25 year return period amounts (Q2, Q10, Q25) and were calculated empirically based on the annual maximum daily discharge values.

2.3. Classification: flood types

The two most important considerations in clustering flood types are the selection of meteorological indices, and how to cluster the flood events based on these indicators. Flood types in mountainous catchments include different combinations of intense-short-duration rainfall, high antecedent rainfall decreasing catchment storage, and snow cover and melt (Merz and Blöschl, 2008). The clusters should reflect these types, and therefore indicators should be able to capture differences.

The indicators representing four different components of flood generation were: 1) short (1-day) duration precipitation, 2) antecedent precipitation over two or more days preceding the flood event, 3) daily and antecedent 2 m temperature, both absolute values and normalized temperature values based on time of year, and 4) day of the year (DOY). The precise antecedent precipitation and temperature indicators were selected based on their correlation with daily discharge. The period of antecedent precipitation that had the highest correlation with discharge was selected, varying the period for two to 60 days before the flood. Temperature in combination with precipitation may identify rainfall as opposed to snowfall, while warm spring temperatures indicate snowmelt, and high temperatures in summer and autumn the possibility of convective precipitation. DOY could indicate possible snow cover and snowmelt, or other seasonally varying phenomena. For temperature, the period was allowed to vary from 1 to 60 days, using both absolute and normalized values due to the strong seasonal signal. Temperature was normalized (T_{mn}) on a daily basis using:

$$T_{mn}=\frac{T_m-\overline{T}_m}{s} \tag{1}$$

where T_m is the daily mean temperature, $\overline{T}_m$ is the average daily mean temperature for all values for the same day of the year, and s is the standard deviation for all values for the same day of the year.

To cluster the flood events into different types the indicators were analyzed by k-means clustering. K-means clustering is an unsupervised clustering technique that separates events into different groups based on one or more indicators. Previous uses include classification of groups of catchments with similar precipitation and flood regimes (Parajka et al., 2010), as well as classifying atmospheric circulation patterns (Huth et al., 2008). The iterative process groups each event into the cluster with the closest centroid, after which the centroid is recalculated based on the mean values of all the events in the cluster. When using multiple indicators for clustering, those with a larger variance will have a larger influence on the center clusters, which can be mitigated by standardizing the indicators. The flood types were clustered for each return period (Q2, Q10 and Q25) using two to all four indicators.

The silhouette index (SI, Rousseeuw, 1987) was used to evaluate the quality of the flood type clusters and determine the final number of clusters. The SI for each cluster can be calculated using:

$$SI=\frac{1}{n_c}\sum_{i=1}^{n_c}\frac{b_i-a_i}{\max\ (a_i,\ b_i)} \tag{2}$$

where n_c is the number of flood events in cluster, b_i is the average Euclidean distance between an observation i and all observations in the next closest cluster, and a_i is the average Euclidean distance between i and all other flood events in the same cluster. SI values vary between 1 and −1, with positive values when they are likely to be correctly classified, negative when the likely belong in another cluster, or near zero for no particular cluster.

The final flood type classification was selected based on the classification with the highest average SI value from (2). It is possible that particular flood types are not observed at all return periods, or there may not be a clear distinction between the more frequent flood types. Therefore, for each study area the final flood type cluster indicators and number of clusters/types were allowed to vary between return periods.

Two different approaches were applied to assess how the flood types may change in the future. For both approaches, 1200 years of future discharge were generated using weather generator enforced by the future climate projections for temperature and precipitation and the HBV model. The first approach was to detect changes in the distribution of historical flood types as a change in dominant flood type may have an impact on the vulnerability or exposure of an area to flooding. To assess the change in distribution, the flood events (Q2, Q10, Q25) were identified based on the historical discharge amounts, allowing the relative change in number of flood frequency to be calculated. The future flood events were placed in the closest historical cluster. A change in the distribution of flood events between the clusters indicates possible changes in the dominant flood type or types in the future.

The second approach repeated the flood type classification using future discharge to allow for new flood types to emerge. To maintain the same number of flood events for clustering, the discharge return periods are re-calculated based on future discharge. The clustering is repeated, based on the four indicators and average SI value. Both the number and the characteristics of the flood types can be compared to the historical flood types to assess changes in future flood type characteristics. The projected temperature values were normalized

based on the historical time series, so as to be able to assess the difference in temperature between the historical and new future flood types.

3. Study area

Two study areas were selected to demonstrate the applicability of the methodology under different conditions: the Ubaye catchment (548 km^2) in the southern French Alps and the Salzach catchment (4637 km^2) in Austria (Fig. 1). Both are located in the European Alps, a region that has warmed twice as fast as the mean temperature for the Northern Hemisphere (Auer et al., 2007). The Alps have also experienced a general retreat of glaciers, an poor snow conditions for winter tourism, with future changes in discharge predicted to increase in winter and decrease in summer (Beniston et al., 2011). Currently, the Ubaye catchment has a mountainous Mediterranean climate with snow on the upper reaches of the catchment for approximately six months of the year (Remaître et al., 2011). It has an observed average annual precipitation between 730 mm and 985 mm with the average annual daily maximum precipitation between 46 mm and 53 mm. As Salzach is located on the north side of the Alps, it has a predominately Alpine climate experiencing annual maximum precipitation and flood maxima generally in summer (Parajka et al., 2010). The Salzach catchment has an observed average annual precipitation varies between 1096 mm and 2035 mm, while the average annual daily maximum precipitation is between 45 mm and 84 mm..

Salzach and Ubaye catchments differ in size and average annual precipitation, they also differ in flood seasonality as shown in previous flood hazard studies (Salzach: Stanzel et al., 2008, Ubaye: Ramesh, 2013). The Ubaye River generally experiences spring flood events, where warm rain amplifies elevated river levels due to snow melt (Ramesh, 2013). Summer flood events are more common for Salzach catchment, which includes the August 2002 flood event where the discharge was the highest in the previous 100 years (Ulbrich et al., 2003). More recently in June 2013, the Salzach catchment recorded high discharge after four days of high precipitation with high antecedent soil moisture (Blöschl et al., 2013).

4. Data selection

The Ubaye and Salzach catchments are covered by a hydrological network with more than 20 years of measurements. The Ubaye catchment contains four rain gauges and measurements of mean daily discharge covering the period 1971–2004. Observed gridded data from the ENSEMBLES project was used for temperature (E-OBS -Haylock et al., 2008), due to missing data and discontinuities in the temperature record for the catchment. E_OBS data have been successfully used in previous flood related studies (e.g. Freudiger et al., 2014; Ionita et al., 2014). The Salzach catchment contains 18 rain gauges, three temperature gauges, and measurements of mean daily discharge for the period 1987–2010. For input into the HBV model the arithmetic mean of multiple temperature station was used for Salzach as it resulted in higher model efficiency coefficients compared to using a single, centrally located, temperature gauge. To calibrate the HBV model, a ten year period was selected (Salzach: 2001–2010, Ubaye: 1995–2004). The validation period was for Salzach: 1988–1997, and for Ubaye: 1971–1980. Both calibration periods contained significant flood events, 2002 in Salzach and 2003 in Ubaye.

For future flood type analysis over the period 2070–2099, four future projections were selected from a set of 15 future climate projections. Four projections were selected to analyze future flood types to maintain a manageable number of future projections, as well as using many projections can tend to highlight the central tendency, rather than extreme conditions (Raff et al., 2009). The full set of 15 originate from the EURO-CORDEX dataset (Jacob et al., 2014). Model output from three RCMs (SMHI-RCA4, DMI_HIRHAM5, KNMI-RACMO22E) driven by 4 different GCMs (ICHEC-EC_EARTH, MOHC-HadGEM2_ES, IPSL-CM5a_MR, MPI-ESM_LR) and two representative concentration pathways, RCP4.5 and RCP 8.5, were selected to cover a wide range of genealogy (Knutti et al., 2013). Details on these 15 projections can be found in the Supplementary material. From the set of 15, four projections were selected using the method by Raff et al. (2009). This method is based on the mean temperature and precipitation projected changes compared to the historical period, averaged over the catchment. Mean changes in temperature and precipitation were used so that the results are not biased towards one particular flood type, for example through selecting

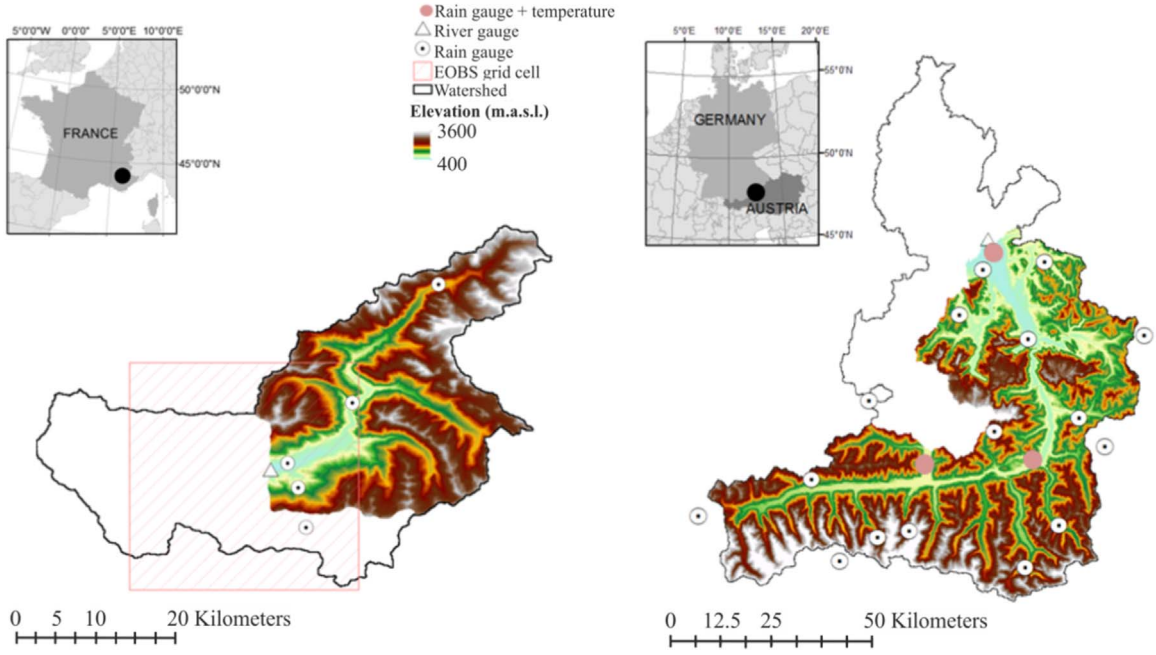

Fig. 1. Map of the two study areas with the location of the rain and river gauges, including location where temperature was also measured. The size and location of the EOBS grid cell is also shown for Ubaye.

changes in extreme precipitation or spring temperature. The selected projections represent combinations of warmer, milder, drier and wetter conditions for time period 2070–2099.

A bias correction method was utilized for the four selected projections for each catchments, as model biases may still remain in RCM data even though they reasonably reproduce meso-scale atmospheric features (Frei et al., 2006). For this work, an empirical-quantile mapping technique (EQM) was chosen. The bias correction methodology for precipitation was based on Themeßl et al. (2012), which has been successfully applied in hydrological climate impact studies (e.g. Dobler et al., 2012; Finger et al., 2012). EQM transforms the empirical cumulative density distribution of the RCM data to match the observed empirical distribution, requiring no assumption about underlying distributions. The bias-correction method performed better than other methods in a range of mid-latitude climates, although may be subject to over-tuning (Lafon et al., 2013).

From Themeßl et al. (2012), the corrected precipitation amounts (Xcorr) can be calculated using:

$$Xcorr_{t,i}=Xraw_{t,j}+CF_i \quad (3)$$

$$CF_i=ecdf_i^{obs,-1}(P_{m,j})-ecdf_j^{mod,-1}(P_{m,j}) \quad (4)$$

$$P_{m,j}=ecdf_j^{mod}(Xraw_j) \quad (5)$$

where $Xraw_{t,j}$ is the precipitation amount on day t at point j, $Xcorr_{t,i}$ is the corrected RCM precipitation amount on day t for gauge i, CF_i is the correction factor at j with regards to i, and P is the probability of Xraw based on the empirical cumulative distribution (ecdf) for daily precipitation values.

The correction factors were calculated monthly, as RCMs biases may differ between seasons (Frei et al., 2006), as well as to align with the weather generator (Section 2.1). Time periods should be longer than 20 years, because for shorter periods results become sensitive to the precise time period chosen (Wood et al., 2004), although results for longer time periods are increasingly likely to contain non-stationeries over the period. The average correction factor for the five most extreme values was used for any unobserved extreme precipitation value.

5. Flood typing

The generated time series from the combination weather generator and HBV model are described in Section 5.1, including the results for the observational period as well as the future projections. These time series form the base for the classification of flood types along with the indicators selected using the historical data. As the catchments have different flood characteristics, the applicability of the flood type classification is shown per catchment (Ubaye in Section 5.2 and Salzach in Section 5.3) for past and future climates.

5.1. Data input for classification

5.1.1. Historical period and indicators

The generated discharge, precipitation and temperature for the historical period in both catchments are characterized in Fig. 2. The discharge time series was generated after calibrating the HBV model. The average Nash-Sutcliffe efficiency (Nash and Sutcliffe, 1970) is computed as performance indicator for the HBV model for was 0.87/0.82 for Salzach and 0.82/0.74 for Ubaye for the calibration/validation period. As the HBV model has been tested for both catchments, details on comparison with observational records can be found in Breinl (2015)..

In the Ubaye catchment, the average daily precipitation was stable thought the year (1–2 mm) with a small peak in October/November (3 mm). In the Salzach catchment there was a clear seasonal signal, with the average daily precipitation lowest in December and January (2 mm) and increasing to 6–7 mm in July and August. The temperature shows the same annual variation for the two regions, with a higher maximum average temperature in the Salzach catchment. As a representation of extreme precipitation for the two catchments, the average annual maximum daily precipitation from the weather generator was 45.2 mm for Ubaye and 42.3 mm for Salzach.

The mean daily discharge for the Ubaye catchments peaks in the spring, with a second smaller peak in the autumn. The second peak aligns with the peak precipitation period, while the first discharge peak may be associated with snowmelt. For the Salzach catchment, the mean discharge and precipitation are highest from late spring to early autumn. An increase in discharge around April/May, not matched in the mean precipitation amounts, was likely caused in part by snowmelt. Higher discharge values in the Salzach catchment could be explained by the difference is size compared to the Ubaye catchment.

The selection of exact indicators was based on the correlation with discharge using the generated time series of precipitation, temperature, and discharge (Fig. 2). Different antecedent periods were tested as indicators in both catchments. The 15-day total precipitation and 5-day normalized temperature had the highest correlation with discharge for the Salzach catchment (correlation coefficients of 0.61 and 0.60 respectively). For the Ubaye catchment, the antecedent period used for precipitation was 35 days and 4 days for normalized temperature (both with a correlation coefficient of 0.42). As the antecedent normalized temperature had a higher correlation with discharge for both study areas, it was used as a potential indicator instead of absolute temperature values. Table 1 lists the potential indicators for the classification of flood types.

5.1.2. Future period

The mean changes in precipitation and temperature in each catchment for 15 different bias-corrected climate projections are shown

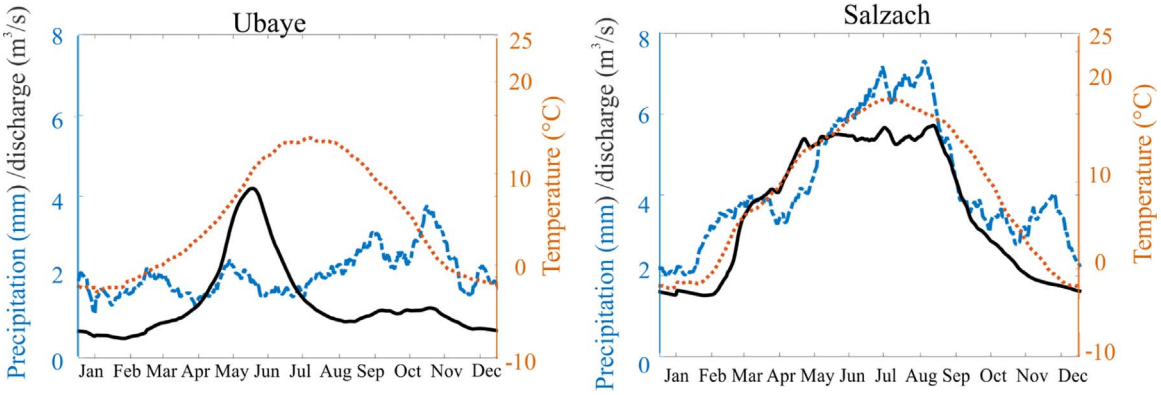

Fig. 2. Mean daily discharge (solid black) from the HBV model, with mean temperature (red dots) and precipitation (blue dash) from the weather generator. Left: Ubaye for the period 1988–2010. Right: Salzach for the period 1971–2004.

Table 1
Potential indicators for classification of flood types for the Ubaye and Salzach catchments.

	Description	Definition	
		Ubaye	Salzach
RR	Short precipitation	1-day total (mm)	1-day total (mm)
RRa	Antecedent precipitation	35-day total (mm)	15 day total (mm)
Tna	Temperature	4 day mean temperature (normalized)	5 day mean temperature (normalized)
DOY	Day of the year	Days from 31st Dec	Days from 31st Dec

in Fig. 3. All projections show an increase in the average annual temperature for the future (2070–2099) compared to the historical period (Ubaye: 1971–2004, Salzach: 1987–2010). The largest increase in temperature for both study areas was more than 2.0% using the MOHC-HadGEM2_ES- SMHI-RCA4 combination. For precipitation, the Ubaye catchment shows most projections with drier conditions, while for Salzach most projections show the area becoming wetter. To reduce the number of future projections, four were selected for each study area using the method proposed by Raff et al. (2009). The SMHI-RCA4 runs with ICHEC-EC_EARTH as driving GCM were selected for both catchment (red circle Fig. 3), with the DMI_HIRHAM5 and ICHEC-EC_EARTH as the other model combination for Ubaye, and SMHI-RCA4 and IPSL-EM5a_MR for Salzach..

The eight projection circled in red were then fed to the weather generator and HBV model to produce four times 1200 years of generated data for both the Ubaye and the Salzach catchments. Fig. 4 shows the mean daily precipitation, temperature and discharge per projection for the period 2070–2099. For Ubaye, all projections had the highest mean precipitation amounts in September and October, extending into August under the Wd projection. Furthermore, besides Wd, the other projections showed a clear seasonal variation in precipitation with two peaks: one in September-October (3–6 mm/day) and a second minor peak in March – May (2–3 mm/day). The temperature had the same annual variation as in the historical period, although warmer by 1–2 °C, except for the winter temperatures for the two warmer projections (Wd and Ww). For the Wd and Ww projections, the temperature was 5–7° higher than in the historical period elevating the mean temperature to above freezing. The changes in temperature and precipitation led to a smaller spring discharge peak than observed in the historical period, particularly for the Wd projection, and higher discharge amounts from October to November..

For Salzach, the seasonal variation of mean precipitation varied between the four future projections in Fig. 4, with the Md projection being most similar to the historical period. The Mw and Ww projections had an increase in the average daily precipitation of 7–8 mm for July and August. For the Wd projection, there were two precipitation peaks of 5–6 mm, one in February to March and the other in June to September. The temperature showed a similar distribution as the historical period with a 2–4 °C increase for the milder projections, Md and Mw, and a 4–6 °C increase for the warmer projections, Wd and Ww. For future discharge, the amount either stayed the same or increased for March to April, with lower discharge between June and October. There was a second discharge peak in three of the projections occurring in July to August for Mw and Ww projections and September to October for the Md projection.

5.2. Ubaye flood types

5.2.1. Historical period (1971–2004)

Per return period the dominant flood types in Ubaye catchment were determined for the historical period 1971–2004. The indicators that independently gave the highest correlation with discharge were: 1-day precipitation (RR), antecedent 35-day precipitation (RRa), and antecedent 4-day normalized temperature (Tna) in combination with the day-of-year (DOY). Only the temperature indicator was normalized, as it was found that normalization of all the indicators resulted in poor separation of clusters (not shown). Fig. 5 shows the flood types where DOY versus precipitation is plotted (a) as well as the silhouette value per event (b). For Q2, flood events were classified into two groups: a small cluster later in the year with higher 1-day rainfall amounts (Type 1) and a second larger cluster earlier in the year (Type 2; Fig. 5a). For the Q2 floods, the combination of 1-day precipitation (RR), temperature and day of the year gave an average SI score of 0.94, indicating a near perfect separation between the two groups. Using the same set of indicators and number of clusters, the SI values for Q10 and Q25 were 0.85 and 0.85, respectively. However further analysis on Q10 and Q25 identified a third group that split the Type 1 floods into two smaller clusters. The two clusters also add the antecedent 35-day precipitation as an indicator and provided a more compact range of conditions under

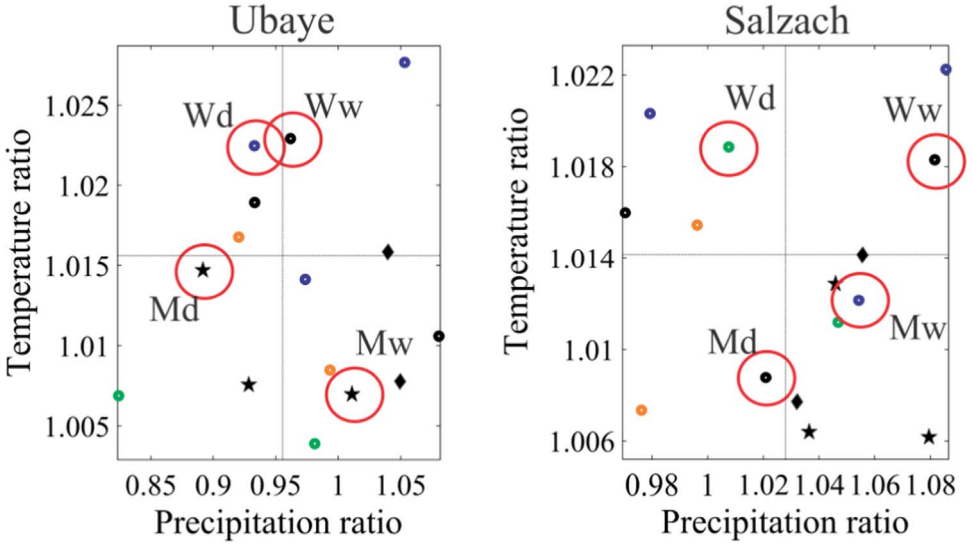

Fig. 3. Projection temperature and precipitation ratio comparing the period 2070–2099 with observational period with Ubaye catchment (left) and the Salzach catchment (right). The selected projections circled in red are for the following combinations: mild dry (Md), mild wet (Mw), warm dry (Wd) and warm wet (Ww). The colors represent the different driving GCMs: black ICHEC-EC_EARTH, blue MOHC-HadGEM2_ES, green IPSL-EM5a_MR, orange MPI-ESM_LR, and the different RCMs are represented with different symbols: circle SMHI-RCA4, star DMI_HIRHAM5, diamond KNMI-RACMO22E.

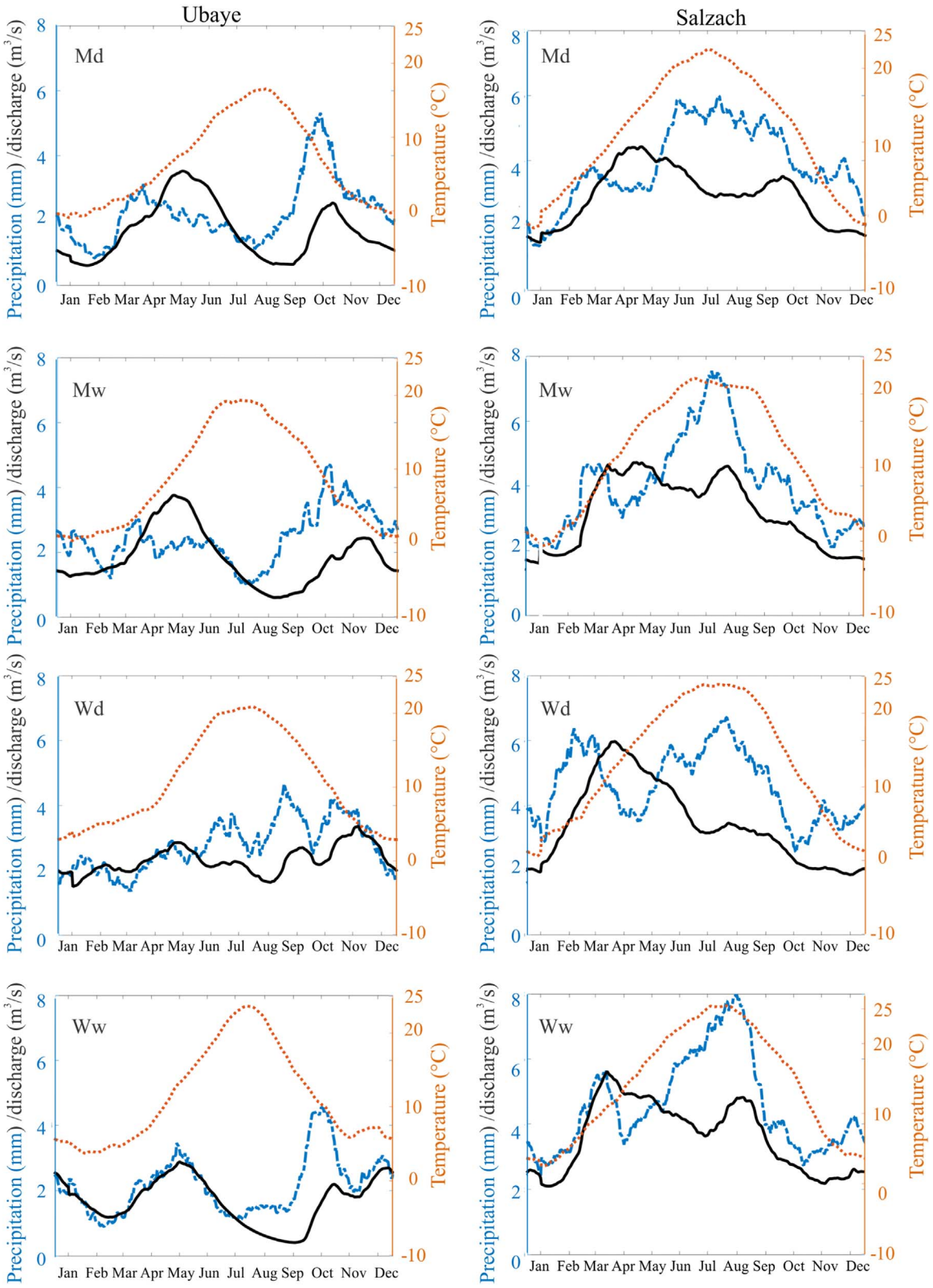

Fig. 4. Mean daily discharge (solid black) from the HBV model, with mean temperature (red dots) and precipitation (blue dash) from the weather generator. Left: Ubaye Right: Salzach. Both for the period 2070–2099 and for each of the four projections Md, Mw, Wd, and Ww.

which the flood events occurred. The average SI score changed to 0.68 for the Q10 floods and 0.73 for the Q25 floods. The majority of individual SI values were above 0.5 in Fig. 5b, indicating that these flood events were most similar to other flood events in their cluster. However, when introducing three flood types some SI values dropped to near zero, particularly for Q10 floods, indicating that there is no preferred cluster for these flood events. The average SI value and cluster center values per indicator are listed in Table 2 per return period and flood type..

For all return periods Type 2 floods occurred between September

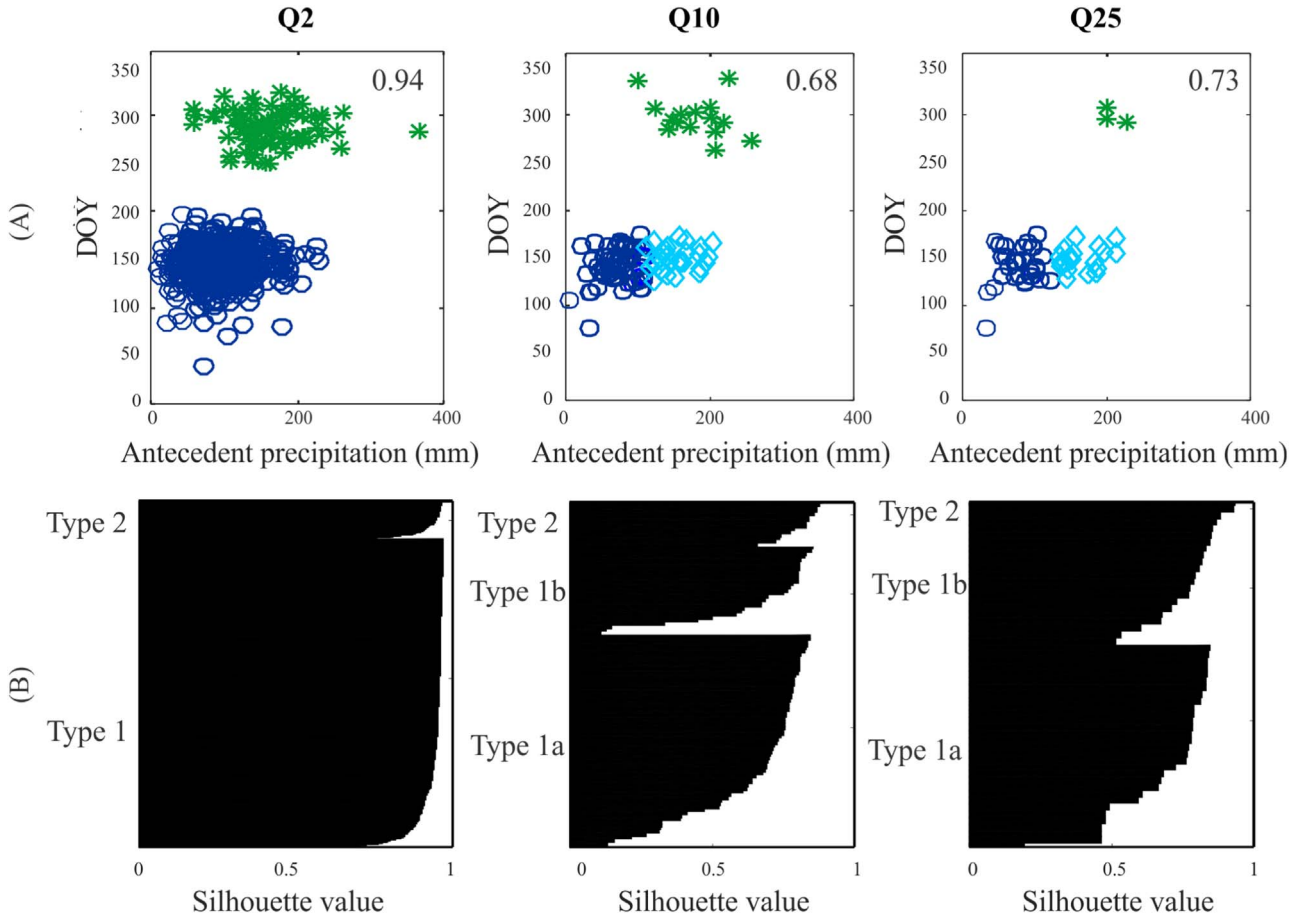

Fig. 5. Clustering of flood types for the Ubaye catchment (A) with the individual silhouette values (B) for the historical period. Green stars indicate Type 2, blue circles Type 1/1a, and light blue diamonds for Type 1b flood events. In each instance, only the antecedent and DOY indicators are shown.

Table 2
Cluster center values for the different flood types for Ubaye under the historical climate. RR is the 1-day precipitation amount, RRa is the 35-day antecedent precipitation and Tna is the normalized 4-day antecedent temperature. The values in bold are used for the cluster centers.

	Ubaye flood types												
	Q2					Q10				Q25			
	RR (mm)	RRa (mm)	Tna	DOY	Type	RR (mm)	RRa (mm)	Tna	DOY	RR (mm)	RRa (mm)	Tna	DOY
Type 1	**15.6**	87	**1.0**	**146**	1a	**30.1**	**71**	**1.8**	**142**	**40.7**	**78**	**1.5**	**141**
					1b	**23.3**	**152**	**0.7**	**150**	**21.7**	**165**	**1.3**	**149**
Type 2	**44.5**	159	**1.5**	**294**	–	**53.2**	**170**	**1.7**	**298**	**45.6**	**210**	**1.9**	**299**

and December with higher than normal temperatures. The warmer temperatures indicated that the rainfall may come from warmer convective events. The associated mean 1-day precipitation amounts are 44.5 mm, 53.2 and 45.6 mm for Q2, Q10 and Q25, respectively (Table 2); values close to the observed annual daily maximum precipitation. The related antecedent precipitation mean values increased with increasing return period indicating higher soil moisture that may lead to more runoff during the short rain events.

Type 1 floods occurred between March and July. Compared to Type 2 floods, Type 1 floods had a lower Tna, but still generally higher than normal (Table 2). The warmer temperatures in spring may have been associated with increased snowmelt, rain on snow, or more rainfall rather than snowfall. The 1-day precipitation amounts for this flood type were lower than for Type 2 floods (Fig. 5a and Table 2), but higher than the mean values in Fig. 2. Therefore it is unlikely that there were snowmelt floods in the Ubaye catchment, a type outlined by Merz and Blöschl (2008), rather, two groups of Rain-Snow floods (here labelled Type 1a and Type 1b) separated by antecedent precipitation amounts. Type 1b floods had higher antecedent precipitation with lower 1-day precipitation compared to Type 1a, as can be seen in Fig. 5 and Table 2. As the temperature indicator covered a shorter time period than the antecedent precipitation, it is not possible to assess whether all the precipitation is snow or rain using the indicators alone. Further investigation of the HBV output data of a select number of the Q25 Type 1b floods showed lower temperatures the preceding weeks, only warming to above normal temperatures in the days before the flood event. In these instances, increased precipitation likely built up the snowpack, especially at higher elevations, which eventually melted and increased the discharge levels. Type 1 floods accounted for more than 90% of the flood events in the generated time series, with an equal split between Type 1a and Type 1b for Q10 and Q25.

As a performance check, the characteristics of the above generated flood types were compared with real floods documented in the catchment. The highest measured discharge amount between 1970

and 2010 was in May 2008, and had similar values for the indicators as the flood Type 1a for Q25. The recorded 1-day precipitation was more than 40 mm at the rain gauges in Fig. 1, with above normal temperature. Considering high observed discharge events, most Q2 events occurred during the March to July period, with only three events that could be classed as Type 2 events. Based on the observed times series, it was not possible to discern Type 1a and Type 1b floods, as there were only four measured Q10 floods and one Q25; too few to cluster. The comparison shows that types of floods captured by the flood classification method appear to be similar to those observed in the Ubaye catchment.

5.2.2. Future flood types (2070–2099)

The future flood types were first analyzed for changes in the flood type frequency compared to the historical period (approach 1). Fig. 6 shows the relative change in number of flood events for each flood type and return period with the historical period (H) as reference (the grey band indicating the 99% random sampling range of historical time series). For Ubaye, all four projections for Q2, Q10, and Q25 events had in increase in overall flood frequency in 2070–2099, as the total length of each bar is greater than the grey horizontal band in Fig. 6. The overall increase was due to a strong increase in the number of Type 2 floods (green) for all projections: a flood type that accounted for less than 10% of the events in the historical period. The increase in these events primarily came from an increase in the 1-day precipitation during autumn (see Fig. 4). There was no consistent change projected in Type 1 for Q2 and Types 1a and 1b for Q10 and Q25. Overall, there was a potential shift in flood types from Type 1 to Type 2 floods..

In the second approach, future flood type clusters were re-classified to account for potential changes in the climate of the catchment that alter the flood types themselves. The center values of the clusters are in Table 3 for each projection (Wd, Ww, Md and Mw). Fig. 7 shows the clustering of flood types based on the indicators DOY and 1-day rainfall for each return period and climate scenario. The individual SI values for Ubaye are in the Supplementary material..

The future flood types in Ubaye were similar to the historical period, except for projection Wd (Fig. 7). Under Wd, Q2 events occurred throughout the year, as opposed to the defined spring and autumn periods observed historically. The three projections Mw, Ww, and Md showed two distinct periods of the year with flood events, as seen with the separation in the DOY between the Type 2 and Type 1 floods in Fig. 7. Under the Md projection, Type 2 could be split for Q10 and Q25 floods, where Type 2a experienced higher 1-day precipitation amounts and lower antecedent precipitation than Type 2b flood events (Fig. 7a and Table 3). All four future projections resulted in fewer Type 1 floods and a separation could no longer be made between Type 1a and 1b floods as in the historical period. For the Q2 events, the average SI value was similar to the historical period, while Q10 and Q25 had higher average SI values than in the historical period, indicative of a clearer separation between the future flood types.

Although similar clusters were detected in the future for the Ubaye catchment, shifts in timing and cluster center values for indicators were projected. The two warmer projections (Wd and Ww) had the Type 1 flood types occurring earlier in the year than historically (on average in March, as opposed to May from the simulated flood events or the May 2008 flood event). Type 2 floods occurred on average at the same time of the year as found in the historical data, although some of the Q2 floods occur in December in all projections (Fig. 7), which was not seen in the historical period (Fig. 5a). For all projections, the cluster center values for 1-day precipitation were higher (Table 3) than the historical values (Table 2). The antecedent precipitation values were lower. All temperature values were on average much warmer than in the historical period, consistent with a warming climate.

5.3. Salzach flood types

5.3.1. Historical period (1987–2010)

For each return period the dominant flood types in the Salzach catchment were determined for the historical period 1987–2010. The indicators that gave the highest correlation with discharge were 1-day precipitation (RR), antecedent 15-day precipitation (RRa), and antecedent 5-day temperature (Tna). Fig. 8 shows the DOY and precipitation per flood event (a) as well as the silhouette value for each event (b). For the Q2 floods using all four indicators, there were two flood types from the classification. The first type were flood events earlier in the year with warmer than normal temperatures and moderate 1-day precipitation (Type 1). A second type occurred later in the year with higher 1-day precipitation and normal or colder than normal temperatures (Type 2; Fig. 8a). The average SI value for this classification was 0.68. The separation between clusters became more distinct for the Q10 and Q25 flood events, with average SI values of 0.84 and 0.74 respectively. Antecedent precipitation was also not used for the Q10 and Q25 events to classify the clusters, due to lower SI values (0.79 and 0.44 respectively if included). For the Q25 flood events, the Type 2 events could be split into two clusters, ones with lower 1-day precipitation amounts and cooler temperatures that occurred earlier in the year (Type 2a) and flood events with higher 1-day precipitation amounts and temperatures near normal (Type 2b). Most of the silhouette values imply a good fit with values above 0.5 in Fig. 8b, however, especially for Q2 events, there are near zero values, demon-

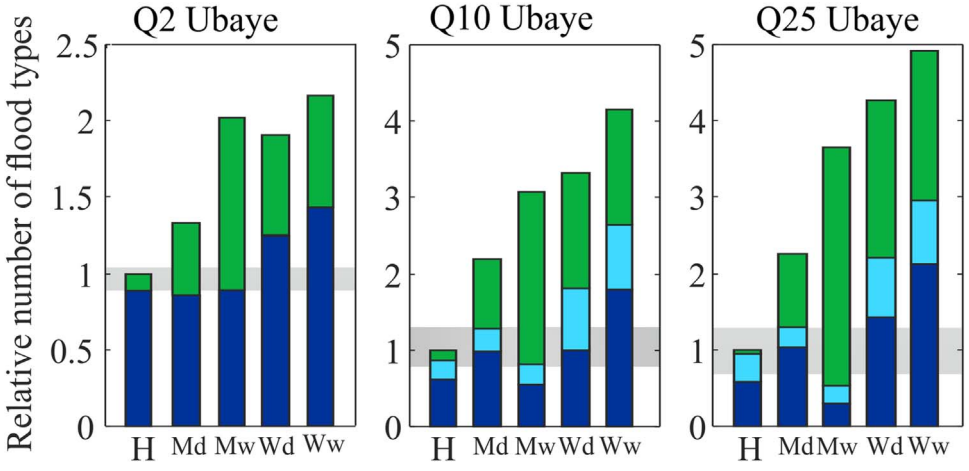

Fig. 6. Approach 1: Number of high discharge events relative to the historical period, split into flood type (blue=Type 1/1a, light blue=Type 1b, green=Type 2, H=for the historical period). The horizontal grey box indicates the 99% random sampling range from the historical period. Amounts above 1 indicate an increase in overall flood frequency and below 1 represents a decrease. The Q2, Q10, Q25 refer to the discharge amount in the historical period. Md, Mw, Wd, and Ww correspond to the projections selected in Fig. 3.

Table 3
New cluster centers for future flood types in the Ubaye catchment (2070–2099) for the four future projections. RR is the 1-day precipitation amount, RRa is the 35-day antecedent precipitation and Tna is the normalized 4-day antecedent temperature. The values in bold are used for the cluster centers.

		Q2				Q10					Q25			
		RR (mm)	RRa (mm)	Tna	DOY	Type	RR (mm)	RRa (mm)	Tna	DOY	RR (mm)	RRa (mm)	Tna	DOY
Mild, dry	Type 1	**32**	105	**1.9**	**122**		**62**	110	**2.2**	**114**	**77**	123	**3.0**	**108**
	Type 2	**66**	148	**1.8**	**285**	2a	**137**	98	**1.7**	**261**	**140**	146	**2.0**	**264**
						2b	**58**	219	**2.3**	**297**	**63**	249	**1.9**	**290**
Mild, wet	Type 1	**36**	84	**2.9**	**115**		**56**	90	**2.9**	**105**	**60**	102	**3.1**	**97**
	Type 2	**51**	167	**2.8**	**296**		**57**	204	**3.0**	**293**	**56**	239	**3.1**	**295**
Warm, dry	Type 1	**43**	101	**4.1**	**90**		**51**	95	**4.4**	**47**	**50**	153	**4.5**	**11**
	Type 2	**51**	168	**3.6**	**303**		**68**	189	**3.7**	**311**	**71**	208	**4.0**	**308**
Warm, wet	Type 1	**51**	99	**4.1**	**67**		**63**	121	**4.6**	**45**	**69**	143	**4.7**	**47**
	Type 2	**55**	171	**3.5**	**303**		**62**	219	**3.9**	**297**	**63**	242	**3.8**	**299**

strating that some flood events did not clearly fit in a particular flood type. The average SI value and cluster center values for each of the indicators are listed in Table 4..

For all return periods, the Type 2 flood events occurred between July and October, with the Type 2a events occurring between July and August and the Type 2b between August and October (Q25 only). All Type 2 floods had on average 1-day precipitation amounts higher than the average annual daily maximum, except for the Type 2a events that were slightly lower (Table 4). The temperature was generally cooler than normal for these events, indicating that the rainfall may have originated from low pressure systems, rather than local convection. However, for the Type 2b events, the temperatures were on average near normal, possibly due a more balanced mixture of synoptically driven rainfall triggered flood events and local convective rainfall triggered flood events. Overall the Type 2 flood events were the dominant flood type in the simulated time series for Salzach, accounting for more than 65% of the flood events.

Type 1 flood events occurred between March and July, with most of the Q10 and Q25 floods occurring between March and May. The average 1-day rainfall and antecedent precipitation were the same between the three return periods for this type, with the 1-day rainfall between 30 and 36 mm higher than normal for this time of year, but lower than the average annual daily maximum. The 15-day antecedent precipitation was on average 135–155 mm, double the average amount. The temperature was warmer than normal for all Type 1 events (Table 4), indicating that warmer temperatures in spring may be associated with increased snowmelt, or more rainfall rather than snowfall, as in Ubaye. The cluster center values for the temperature indicator also increased with increasing return period (Table 4), indicating either more snowmelt, or more rapid snowmelt. Overall the Type 1 flood events accounted for 10–35% of the total Q2, Q10, and Q25 floods in the Salzach catchment.

The characteristics of the generated flood types was compared with real flood events document in the Salzach catchment. For the August 2002 flood event, the 1-day rainfall amounts in some places exceeded the 100-year return level period, with heavy precipitation also recorded in the weeks before the event (Ulbrich et al., 2003). These are characteristic of the Type 2 flood events described in Table 4 and Fig. 8a, although slightly earlier in the year than average for the simulated data. More recently the early June 2013 flood occurred after three days of heavy precipitation combined with high antecedent moisture conditions in part due to snow melt (Blöschl et al., 2013). This flood bares resemblance to the Type 1 flood events, where snowmelt appears to play a role, alongside heavy precipitation and higher than normal antecedent precipitation. Overall, the flood types captured through the classification of generated data appear to be similar to the observed flood types.

5.3.2. Future flood types (2070–2099)

The change in frequency of each of the flood types was analyzed first (approach 1). Fig. 9 shows the relative change in number of flood event for each flood types and return period compared to the historical period (H). For each return period, three projections of flood events show an increase in overall frequency, with only the Md total bar length below the grey horizontal band in Fig. 9. The Md projection was also unique between projections for the individual flood types, where the milder, drier projection had a decrease in Type 2 flood events and no change in the Type 1 flood events. For the other three projections, Mw, Wd, Ww, each flood type had an increase in frequency, although the increase was small for Type 2a events for the Q25 Mw projection. For all return periods, the Type 1 flood events had the greatest increase in frequency, becoming the dominant flood type. For the two warmer projections, Wd and Ww, there were still more Type 2 flood events than Type 1. Overall the results for the Salzach catchment show that the distribution of flood types may shift to more events earlier in the year, although Type 2 flood types remained the dominant type, except in the Mw projection..

In approach 2, the future flood types were re-classified to account for possible changes in flood type characteristics by 2070–2099. The center values for the indicators for each projection (Md, Mw, Wd, Ww) and return period are in Table 5. Fig. 10 shows the clustering of flood types based on the indicators DOY and 1-day rainfall, with the individual SI values in the Supplementary material..

For Salzach there was a larger difference between the historical and future flood types compared with Ubaye. The most similar flood types from the Md projection retained the Type 1 and Type 2 events, although they occurred over a larger portion of the year (Fig. 10a). The Mw projection future flood type characteristics had the largest contrast from the historical period (Fig. 10b). This was the only projection that did not use DOY in all of the flood type classifications (Table 5). Four flood types were identified for Q2 events based on only temperature and 1-day precipitation, with the flood events that had the highest 1-day precipitation and coldest normalized temperature occurring in spring. Only two flood types were defined for the Q10 events, one group only occurring in spring, with higher 1-day precipitation values, and a second group that occurred throughout the year with higher antecedent precipitation. For the Q25 flood events, three types were identified with the inclusion of the DOY indicator. For the two warmer projections, Wd and Ww, between two and four clusters were found based on 1-day precipitation, temperature, and DOY with higher 1-day totals (Fig. 10c, d). Flood types 2a and 1 were similar to the flood types 2 and 1 from the historical period. However, in both cases a third type, Type 2b, was also observed, occurring in November and December with abnormally high temperatures, much later in the year than observed in the historical period. For the Wd projection, a fourth type, Type 2c, was also observed and occurred in June. As with Ubaye, all temperatures were higher than normal, as would be expected in a warmer climate.

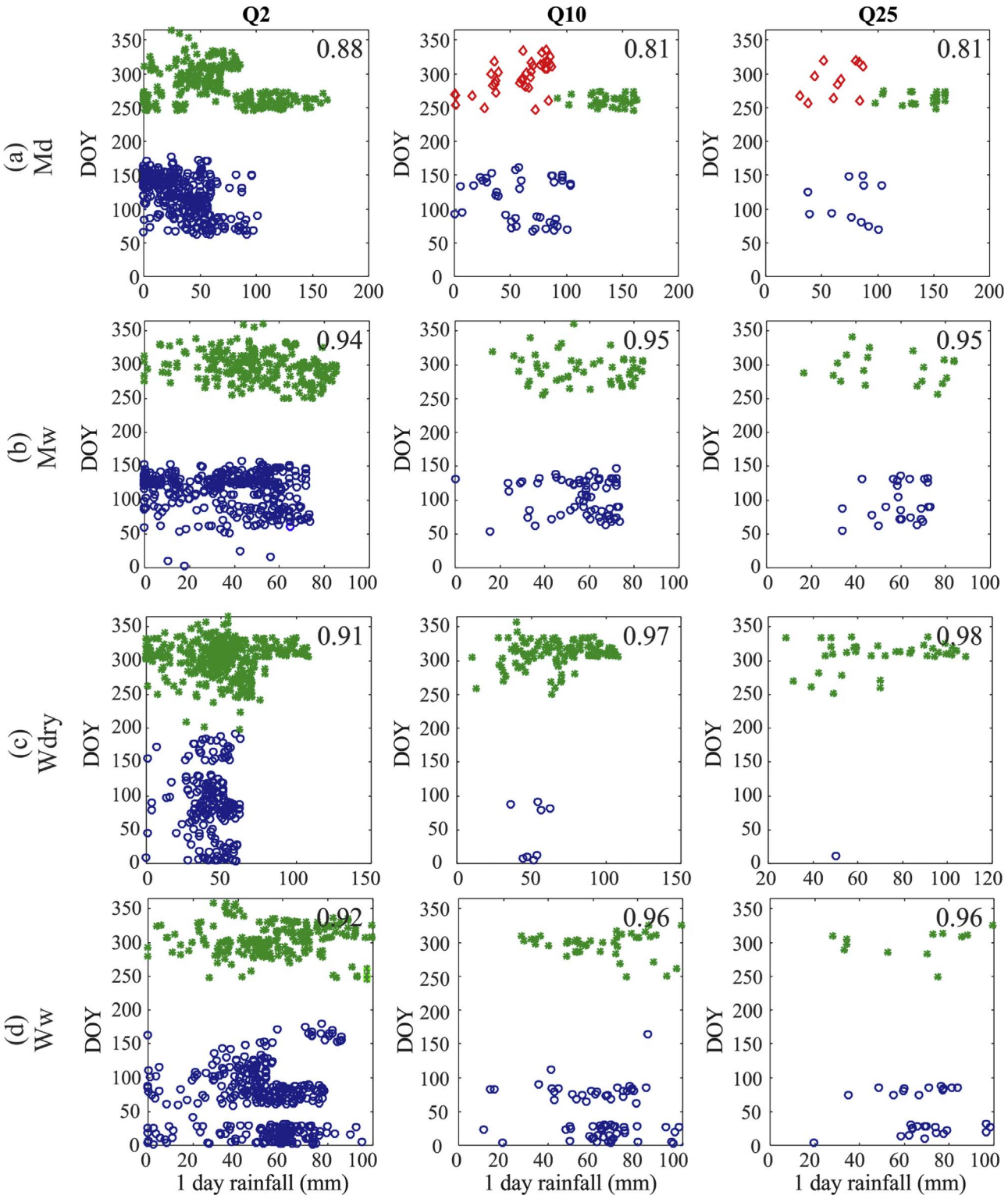

Fig. 7. Clustering of future flood types for the Ubaye catchment for the period 2070–2099 per selected projection. Green stars indicate Type 2 floods, blue circles Type 1 floods, red diamonds for Type 3 floods with indicator 1-day rainfall on the x-axis and indicator DOY on the y-axis two. The average SI value is shown the in top right corner.

6. Discussion

The developed flood type classification methodology was able to define the main historical flood types for both tested catchments as result of temporal data expansion by using weather generator combined with the HBV rainfall-runoff model. Separation between flood types based on the SI value depended on both the catchment characteristics as well as the number of flood events in the cluster. The separation was less clear for lower return period floods (Q2) in the Salzach catchment than Ubaye, which could be linked to the two distinct peaks in the precipitation distribution in Ubaye that were absent in Salzach (Fig. 2). Generally, there was an increase in SI value between the flood types with higher return period, for both catchments and as well as for historical as future periods. A reason could be that more frequent discharge events can occur in a wider range of conditions, while the extreme flood event conditions only occur under

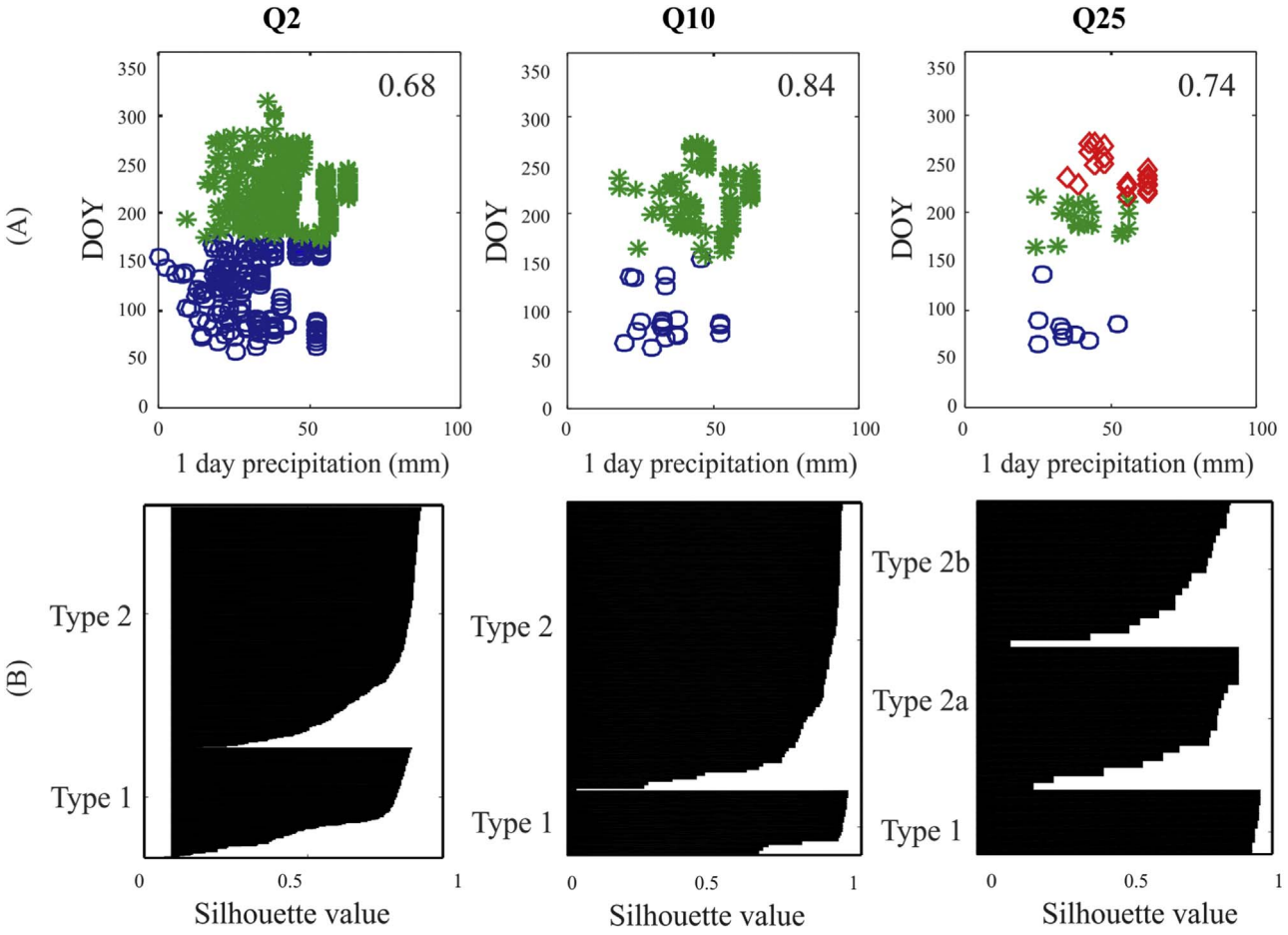

Fig. 8. Clustering of flood types for the Salzach catchment (A), with the individual silhouette values (B). Green stars indicate Type 2/2a, blue circles Type 1, with red diamonds for Type 2b flood events. Only the RR and DOY indicators are shown.

Table 4
Cluster center values for the different discharge magnitudes for Salzach under the historical climate. RR is the 1-day precipitation amount, RRa is the 15-day antecedent precipitation and Tna is the normalized 5-day antecedent temperature. The values in bold are used for the cluster centers.

	Salzach flood types												
	Q2, SI=0.68				Q10, SI=0.84					Q25, SI=0.74			
	RR (mm)	RRa (mm)	Tna	DOY	RR (mm)	RRa (mm)	Tna	DOY		RR (mm)	RRa (mm)	Tna	DOY
Type 1	**31**	**153**	**0.95**	**125**	**35**	137	**1.4**	**94**		**36**	146	**2.0**	**84**
Type 2	**43**	**232**	**−0.27**	**220**	**48**	246	**−0.5**	**215**	2a	**41**	284	**−0.5**	**192**
									2b	**53**	272	**−0.1**	**240**

specific combinations of indicator values, possibly linked to certain atmospheric situations such as atmospheric blocking leading to persistent rain over the catchment.

The developed methodology employs four types of indicators using only time series of temperature, precipitation data from the weather generator and the DOY. The selected indicators have strongest correlation with generated discharge, but could limit the number of flood types. Other flood types, such as snowmelt, may be difficult to capture with only temperature and precipitation indicators (Gelfan, 2010). It is possible that new indicators should be used for clustering future flood events or other catchments. Using other indicators as well as antecedent periods for the temperature, precipitation, and DOY may alter the mean indicator values per flood type, and possibly the flood types themselves. Furthermore, the decision not to standardize all the indicators would have affected the cluster centers as those with smaller variance had a smaller influence on the cluster centers, particularly in this case temperature. During preliminary analysis, standardizing the indicators decreased the performance of the clustering and therefore was not included. For other regions or indicators, however, weighting and standardization of variables may be a viable option where the separation between clusters is less clear. Overall, for both test catchments most of the silhouette values were greater than 0.5, indicating that these two, frequently measured meteorological variables, temperature and precipitation, along with day of the year can be used to distinguish two or three clearly different flood types.

Previous work shows that hydrologic future projections are potentially sensitive to the GCM, RCM, rainfall-runoff model and downscaling method used (e.g. Dobler et al. (2012); Wood et al. (2004)). Here climate model projections were selected based on mean changes in temperature and precipitation (Section 4), although Figs. 6 and 9 do not show consistent changes in flood types between the selections beyond the milder, drier projections showing the least number of flood events. These differences suggest that selecting projections based on mean changes in temperature and precipitation may not directly relate

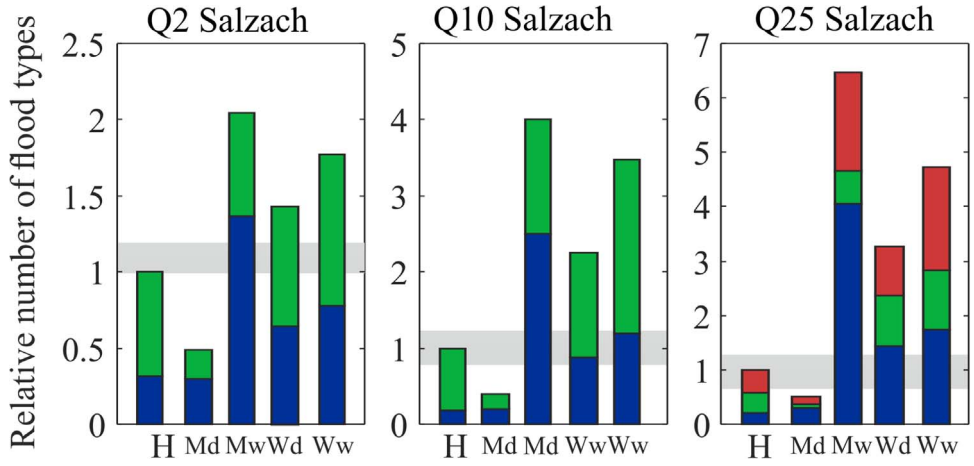

Fig. 9. Approach 1: Number of high discharge events relative to the historical period, split into flood type (blue=Type 1, green=Type 2/2a, red=Type 2b, H=for the historical period). The horizontal grey box indicates the 99% random sampling range from the historical period. Amounts above 1 indicate an increase in overall flood frequency and below 1 represents a decrease. The Q2, Q10, Q25 refer to the discharge amount in the historical period. Md, Mw, Wd, and Ww correspond to the projections selected in Fig. 3.

to the changes in flood types, although selecting the mean values reduces the assumptions on the governing factors for flood events. The selected indicators assume that the GCMs and RCMs were able to project future changes in precipitation, while GCMs are known to have limited skill in capturing factors driving regional precipitation, which would affect future projections of precipitation, and therefore flood types in this study (Asadieh and Krakauer, 2015; Merz et al., 2014). Furthermore, the weather generator assumed no change in autocorrelation, or inter-site correlation, rather focusing on changes in precipitation amounts as well as temperature. Spatial changes in precipitation can in some instances cause greater changes in discharge amounts than temporal changes (Perdigão and Blöschl, 2014). Not changing the autocorrelation might partly explain why the Type 2b floods saw a larger increase in frequency compared to those with larger antecedent precipitation (Type 2a). However, future projections in temperature and precipitation amounts still led to changes in the dominant flood types in a catchment as well as the flood frequency, although the range of future flood frequencies and flood types for the study areas may actually be greater than presented here. A more detailed study in changing flood types for a particular area should possibly consider more projections, as well as changes in land use and other catchment characteristics, as this may also influence future flooding.

Two approaches were provided to assess changes in the flood types under four future climate scenarios. These approaches were complementary to each other as one estimates changes in frequency of the historical flood types, where the second assesses whether future precipitation and temperature would lead to (dis)similar flood types compared to the historical period. Changes in the dominant flood type can have implications for local land use practices. For example, in the Ubaye catchment during summer the flood plains are used for farming and camping, as the historical flood events have occurred during spring. However, if summer and autumn floods become the dominant flood type, as projected in Section 5.2.2, this will have implications for exposure in the area. Changes in the characteristics, as in approach two, are also important, such as the decrease in the temperature indicator for the Type 1 floods in the Mw projection, even under a warmer climate.

Flood types for the historical period may be inherent to the combination of weather generator and specific rainfall-runoff model, enforced by historical observational records of precipitation and temperature. Two flood types were found, Type 1 and 2, which are similar to Rain-Snow and Short Rain floods respectively as classified in Merz and Blöschl (2008). Other flood types listed in the previous work, Snowmelt and Long Rain, were not distinguished through the flood type classification. Instead, in cases where there were three or more flood types, the types generally split one of the main clusters, based on which was the dominant flood type in the catchment. Even when considering the new flood types for 2070–2099 the Rain-Snow and Short Rain floods remained the two clear flood types from Merz and

Table 5
Cluster center values for the different discharge magnitudes for Salzach under the historical climate. RR is the 1-day precipitation amount, RRa is the 15-day antecedent precipitation and Tna is the normalized 5-day antecedent temperature. The values in bold are used for the cluster centers.

		Salzach flood types Q2					Q10					Q25			
		RR mm	RRa mm	Tna	DOY	New Type	RR mm	RRa mm	Tna	DOY	New Type	RR mm	RRa mm	Tna	DOY
(A) Mild, dry	Type 1	**32**	74	**1.6**	**115**		**40**	82	**2.1**	**96**		**44**	95	**2.0**	**92**
	Type 2	**42**	94	**1.1**	**265**		**44**	114	**1.4**	**275**		**47**	123	**1.9**	**281**
(B) Mild, wet	Type 1	**109**	52	**0.6**	74	1	**113**	58	**1.2**	78	1	**101**	164	4.4	**80**
	Type 3a	**24**	115	**1.6**	160		**60**	132	**1.1**	164	2a	**65**	177	4.5	**179**
	Type 3b	**66**	87	**1.3**	167	2									
	Type 3c	**45**	113	**1.3**	193						2b	**55**	217	4.4	**306**
(C) Warm, dry	Type 1	**48**	85	**2.7**	**78**		**58**	114	**2.7**	**75**	1	**62**	141	**2.8**	77
	Type 2					2b	**57**	116	**4.6**	**364**					
		69	103	**2.2**	**237**	2c	**86**	138	**1.6**	**167**	2c	**80**	149	**1.7**	**171**
						2a	**79**	132	**2.3**	**256**	2a	**74**	173	**2.2**	**256**
(D) Warm, wet	Type 1	**51**	75	**2.3**	**84**		**56**	105	**2.7**	**78**		**59**	135	**3.3**	**79**
	Type 2a	**65**	122	**2.7**	**203**		**74**	151	**2.8**	**208**		**75**	186	**2.8**	**212**
	Type 2b	**77**	92	**3.5**	**342**		**118**	102	**3.7**	**352**		**132**	92	**4.0**	**352**

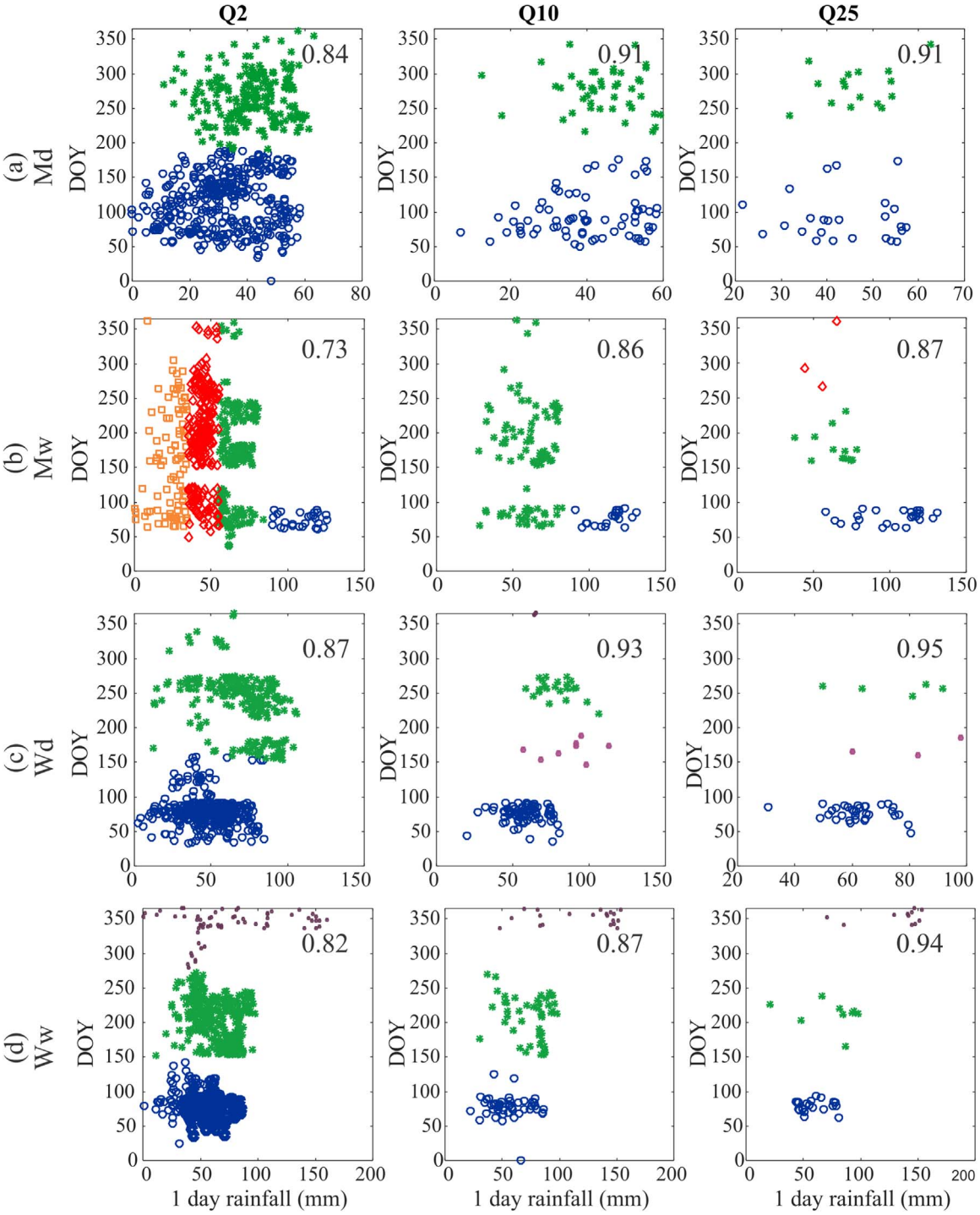

Fig. 10. Clustering of future flood types for the Salzach catchment for the period 2070–2099 per selected projection. In the case of two flood types, green stars indicate Type 2 floods, blue circles Type 1 floods. In other cases, red diamond and orange squares indicate Type 3 floods, and purple stars indicate a subset of Type 2 floods. In each plot shows the indicator 1-day rainfall on the x-axis and indicator DOY on the y-axis two. The average SI value is shown the in top right corner.

Blöschl (2008), even if the characteristics of the flood type were different. It is possible that a flood type, such as Snowmelt, could trigger only discharge with shorter return periods in the catchments, and not generate high discharge levels. The ability of the method to capture snowmelt floods could be confirmed through future work in a catchment where these flood types occurred.

While to the authors knowledge there has been little coverage of changes in future flood types for Alpine catchments, the results found here are similar to other studies for the two catchments. Hall et al. (2014) concluded that an increase in future extreme precipitation events with mean precipitation increases over northern Europe and decrease in southern areas will results in different changes in flood frequency between catchments in the future. For the Ubaye catchment, Saez et al. (2013) hypothesize that future warming could enhance snowmelt during the spring, although from the results in Section 5.2 this appears to be offset by the decrease in antecedent precipitation. The increase in temperature in both Fig. 4 and Table 3 is consistent with future warming in the area (Malet et al., 2007; Rousselot et al., 2012). For the Salzach, previous work found no clear trend in flood frequency (Dobler et al., 2011), although the authors commented that

higher spring temperatures could lead to more frequency flooding events in this season. The similarities between this work and previous studies implies that the even with the limitations of method outlined above the method produces reasonable results using relatively straightforward method.

7. Conclusion

This paper demonstrated a methodology developed for detecting present and future flood types. Long time series of discharge were generated using a weather generator coupled with a rainfall-runoff model to provide sufficient flood events for classification into different causal types. The types were determined to be sufficiently different based on the silhouette index. Future climate scenarios were assessed using bias correction of different RCM climate projections and to train the weather generator. The methodology was applied in two European Alpine catchments, Ubaye and Salzach, for both the historical period, and the future period (2070–2099).

The flood type classification was based on a set of temperature and precipitation indicators as well as day of the year. In this work, the selection of indicators was based on correlation with historical discharge. Our findings showed that the methodology was able to reliably reproduce the observed flood types for the two catchments. Care is needed in the selection of the indicator values however, as the variables used will affect the final flood types.

When looking at the future projections, both study areas showed potential changes in the distribution of flood types, as well as the types themselves. For the Ubaye catchment, flood events may shift from Rain-Snow (Type 1) dominated floods to Short Rain (Type 2), a type that currently accounts for less than 10% of flood events. Re-clustering of flood types shows changes in the characteristics of the flood events, with higher average daily precipitation values and flood events both later and earlier in the year in the future. For the Salzach catchment, Short Rain (Type 2) floods may remain the dominant flood type, although it is possible there is an increase in Rain-Snow floods (Type 1), and overall flood frequency. Re-classifying of the future flood events for this catchment also found changes in the flood type characteristics with events occurring throughout the year, and in some instances particularly higher daily precipitation in spring. Although only a limited number of climate projections were considered, the results showed the potential of the methodology developed to assess the full range of possible future changes in flood types for the catchments.

Therefore, this methodology identifies realistic flood types, and can be used to assess future changes in flood types. The methodology has potential to be applied to higher return periods and other catchments as long as the observational records of precipitation, temperature and flood events are of good quality and length. Changes in flood types are an important consideration for future research as the changes will have an impact on the local social and ecological systems and have implications for future flood management.

Acknowledgements

This research was funded by the FP7 Marie Curie Initial Training Network “CHANGES” under Grant Agreement No. 263953. Data were provided by the Central Institution for Meteorology and Geodynamics (ZAMG), the Federal Ministry of Agriculture, Forestry, Environment and Water Management, and the German Meteorological Service (DWD) and Météo France. We acknowledge the World Climate Research Programme’s Working Group on Regional Climate, and the Working Group on Coupled Modelling. We also thank the climate modelling groups (Supplementary material) for producing and making available their model output.

Appendix A. Supplementary material

Supplementary data associated with this article can be found in the online version at doi:10.1016/j.wace.2016.10.001.

References

Akhtar, M., Ahmad, N., Booij, M.J., 2008. The impact of climate change on the water resources of Hindukush–Karakorum–Himalaya region under different glacier coverage scenarios. J. Hydrol. 355, 148–163. http://dx.doi.org/10.1016/j.jhydrol.2008.03.015.

Alila, Y., Mtiraoui, A., 2002. Implications of heterogeneous flood-frequency distributions on traditional stream-discharge prediction techniques. Hydrol. Process. 16, 1065–1084. http://dx.doi.org/10.1002/hyp.346.

Arnell, N., Gosling, S., 2014. The impacts of climate change on river flood risk at the global scale. Clim. Change, 1–15. http://dx.doi.org/10.1007/s10584-014-1084-5.

Asadieh, B., Krakauer, N.Y., 2015. Global trends in extreme precipitation: climate models versus observations. Hydrol. Earth Syst. Sci. 19, 877–891. http://dx.doi.org/10.5194/hess-19-877-2015.

Auer, I., Böhm, R., Jurkovic, A., Lipa, W., Orlik, A., Potzmann, R., Schöner, W., Ungersböck, M., Matulla, C., Briffa, K., et al., 2007. HISTALP—historical instrumental climatological surface time series of the Greater Alpine Region. Int. J. Climatol. 27, 17–46. http://dx.doi.org/10.1002/joc.1377.

Bárdossy, A., Filiz, F., 2005. Identification of flood producing atmospheric circulation patterns. J. Hydrol. 313, 48–57. http://dx.doi.org/10.1016/j.jhydrol.2005.02.006.

Benestad, R., Haugen, J., 2007. On complex extremes: flood hazards and combined high spring-time precipitation and temperature in Norway. Clim. Change 85, 381–406. http://dx.doi.org/10.1007/s10584-007-9263-2.

Beniston, M., Stoffel, M., Hill, M., 2011. Impacts of climatic change on water and natural hazards in the Alps: can current water governance cope with future challenges? Examples from the European “ACQWA” project. Environ. Sci. Policy 14, 734–743. http://dx.doi.org/10.1016/j.envsci.2010.12.009.

Bergström, S., 1976. Development and Application of a Conceptual Runoff Model for Scandinavian Catchments. Department of Water Resources, Engineering, Lund Institute of Technology, Lund, Sweden.

Bergström, S., Carlsson, B., Gardelin, M., Lindström, G., Pettersson, A., Rummukainen, M., 2001. Climate change impacts on runoff in Sweden - assessments by global climate models, dynamical downscaling and hydrological modelling. Clim. Res. 16, 101–112. http://dx.doi.org/10.3354/cr016101.

Beven, K., 1999. How far can we go in distributed hydrological modelling? Hydrol. Earth Syst. Sci. 5, 1–12. http://dx.doi.org/10.5194/hess-5-1-2001.

Blöschl, G., Nester, T., Komma, J., Parajka, J., Perdigão, R.A.P., 2013. The June 2013 flood in the Upper Danube Basin, and comparisons with the 2002, 1954 and 1899 floods. Hydrol. Earth Syst. Sci. 17, 5197–5212. http://dx.doi.org/10.5194/hess-17-5197-2013.

Booij, M.J., 2005. Impact of climate change on river flooding assessed with different spatial model resolutions. J. Hydrol. 303, 176–198. http://dx.doi.org/10.1016/j.jhydrol.2004.07.013.

Breinl, K., 2015. Driving a lumped hydrological model with precipitation output from weather generators of different complexity. Hydrol. Sci. J.. http://dx.doi.org/10.1080/02626667.2015.1036755.

Breinl, K., Turkington, T., Stowasser, M., 2014. Simulating daily precipitation and temperature: a weather generation framework for assessing hydrometeorological hazards. Meteorol. Appl.. http://dx.doi.org/10.1002/met.1459.

Das, T., Bárdossy, A., Zehe, E., He, Y., 2008. Comparison of conceptual model performance using different representations of spatial variability. J. Hydrol. 356, 106–118.

Delgado, J.M., Merz, B., Apel, H., 2014. Projecting flood hazard under climate change: an alternative approach to model chains. Nat. Hazards Earth Syst. Sci. 14, 1579–1589. http://dx.doi.org/10.5194/nhess-14-1579-2014.

Dobler, A., Yaoming, M., Sharma, N., Kienberger, S., Ahrens, B., 2011. Regional climate projections in two Alpine River Basins: Upper Danube and Upper Brahmaputra. Adv. Sci. Res. 7, 11–20. http://dx.doi.org/10.5194/asr-7-11-2011.

Dobler, C., Hagemann, S., Wilby, R.L., Stötter, J., 2012. Quantifying different sources of uncertainty in hydrological projections in an Alpine watershed. Hydrol. Earth Syst. Sci. 16, 4343–4360. http://dx.doi.org/10.5194/hess-16-4343-2012.

Dube, A., Ashrit, R., Ashish, A., Sharma, K., Iyengar, G.R., Rajagopal, E.N., Basu, S., 2014. Forecasting the heavy rainfall during Himalayan flooding—June 2013. Weather Clim. Extrem. 4, 22–34. http://dx.doi.org/10.1016/j.wace.2014.03.004.

Finger, D., Heinrich, G., Gobiet, A., Bauder, A., 2012. Projections of future water resources and their uncertainty in a glacierized catchment in the Swiss Alps and the subsequent effects on hydropower production during the 21st century. Water Resour. Res. 48, w02521. http://dx.doi.org/10.1029/2011wr010733.

Frei, C., Schöll, R., Fukutome, S., Schmidli, J., Vidale, P.L., 2006. Future change of precipitation extremes in Europe: intercomparison of scenarios from regional climate models. J. Geophys. Res. Atmos. 111, D06105. http://dx.doi.org/10.1029/2005jd005965.

Freudiger, D., Kohn, I., Stahl, K., Weiler, M., 2014. Large-scale analysis of changing frequencies of rain-on-snow events with flood-generation potential. Hydrol. Earth Syst. Sci. 18, 2695–2709. http://dx.doi.org/10.5194/hess-18-2695-2014.

Gaál, L., Szolgay, J., Kohnová, S., Parajka, J., Merz, R., Viglione, A., Blöschl, G., 2012. Flood timescales: understanding the interplay of climate and catchment processes through comparative hydrology. Water Resour. Res. 48, W04511. http://dx.doi.org/10.1029/2011wr011509.

Gain, A., Apel, H., Renaud, F., Giupponi, C., 2013. Thresholds of hydrologic flow regime of a river and investigation of climate change impact—the case of the Lower Brahmaputra river Basin. Clim. Change 120, 463–475. http://dx.doi.org/10.1007/s10584-013-0800-x.

Gao, H., He, X., Ye, B., Pu, J., 2012. Modeling the runoff and glacier mass balance in a small watershed on the Central Tibetan Plateau, China, from 1955 to 2008. Hydrol. Process. 26, 1593–1603. http://dx.doi.org/10.1002/hyp.8256.

Garner, G., Van Loon, A.F., Prudhomme, C., Hannah, D.M., 2015. Hydroclimatology of extreme river flows. Freshw. Biol., 1–16. http://dx.doi.org/10.1111/fwb.12667.

Gelfan, A., 2010. Extreme snowmelt floods: frequency assessment and analysis of genesis on the basis of the dynamic-stochastic approach. J. Hydrol. 388, 85–99. http://dx.doi.org/10.1016/j.jhydrol.2010.04.031.

Hall, J., Arheimer, B., Borga, M., Brázdil, R., Claps, P., Kiss, A., Kjeldsen, T.R., Kriaučiūnienė, J., Kundzewicz, Z.W., Lang, M., et al., 2014. Understanding flood regime changes in Europe: a state-of-the-art assessment. Hydrol. Earth Syst. Sci. 18, 2735–2772. http://dx.doi.org/10.5194/hess-18-2735-2014.

Haylock, M.R., Hofstra, N., Klein Tank, A.M.G., Klok, E.J., Jones, P.D., New, M., 2008. A European daily high-resolution gridded data set of surface temperature and precipitation for 1950–2006. J. Geophys. Res. 113, D20119. http://dx.doi.org/10.1029/2008jd010201.

Huth, R., Beck, C., Philipp, A., Demuzere, M., Ustrnul, Z., Cahynová, M., Kyselý, J., Tveito, O.E., 2008. Classifications of atmospheric circulation patterns. Ann. N. Y. Acad. Sci. 1146, 105–152. http://dx.doi.org/10.1196/annals.1446.019.

Ionita, M., Dima, M., Lohmann, G., Scholz, P., Rimbu, N., 2014. Predicting the june 2013 European flooding based on precipitation, soil moisture, and sea level pressure. J. Hydrometeorol. 16, 598–614. http://dx.doi.org/10.1175/JHM-D-14-0156.1.

Jacob, D., Petersen, J., Eggert, B., Alias, A., Christensen, O., Bouwer, L., Braun, A., Colette, A., Déqué, M., Georgievski, G., et al., 2014. EURO-CORDEX: new high-resolution climate change projections for European impact research. Reg. Environ. Change 14, 563–578. http://dx.doi.org/10.1007/s10113-013-0499-2.

Knutti, R., Masson, D., Gettelman, A., 2013. Climate model genealogy: generation CMIP5 and how we got there. Geophys. Res. Lett. 40, 1194–1199. http://dx.doi.org/10.1002/grl.50256.

Köplin, N., Schädler, B., Viviroli, D., Weingartner, R., 2014. Seasonality and magnitude of floods in Switzerland under future climate change. Hydrol. Process. 28, 2567–2578. http://dx.doi.org/10.1002/hyp.9757.

Kunkel, K.E., Changnon, S.A., Angel, J.R., 1994. Climatic aspects of the 1993 Upper Mississippi river Basin flood. Bull. Am. Meteorol. Soc. 75, 811–822. http://dx.doi.org/10.1175/1520-0477(1994)075 < 0811:CAOTUM > 2.0.CO;2.

Lafon, T., Dadson, S., Buys, G., Prudhomme, C., 2013. Bias correction of daily precipitation simulated by a regional climate model: a comparison of methods. Int. J. Climatol. 33, 1367–1381. http://dx.doi.org/10.1002/joc.3518.

Malet, J.-P., Durand, Y., Remaître, A., Maquaire, O., Etchevers, P., Guyomarch, G., Déqué, M., van Beek, L., 2007. Assessing the influence of climate change on the activity of landslides in the Ubaye Valley. In: McInnes, R., Jakeways, J., Fairbank, H., Mathie, E. (Eds.), Proceedings of the International Conference on Landslides and Climate Change – Challenges and Solutions, Wiley, pp. 195–205.

McCabe, G.J., Hay, L.E., Clark, M.P., 2007. Rain-on-Snow Events in the Western United States. Bull. Am. Meteorol. Soc. 88, 319–328. http://dx.doi.org/10.1175/bams-88-3-319.

Merz, B., Aerts, J., Arnbjerg-Nielsen, K., Baldi, M., Becker, A., Bichet, A., Blöschl, G., Bouwer, L.M., Brauer, A., Cioffi, F., et al., 2014. Floods and climate: emerging perspectives for flood risk assessment and management. Nat. Hazards Earth Syst. Sci. 14, 1921–1942. http://dx.doi.org/10.5194/nhess-14-1921-2014.

Merz, R., Bloschl, G., 2003. Regional Flood Risk-What are the Driving Processes?, Water Resources Systems - Hydrological Risk. Management and Development. IAHS Publ, Sapporo, Japan, 49–58.

Merz, R., Blöschl, G., 2008. Flood frequency hydrology: 1. Temporal, spatial, and causal expansion of information. Water Resour. Res. 44, W08432. http://dx.doi.org/10.1029/2007wr006744.

Nash, J.E., Sutcliffe, J.V., 1970. River flow forecasting through conceptual models part I — a discussion of principles. J. Hydrol. 10, 282–290. http://dx.doi.org/10.1016/0022-1694(70)90255-6.

Nied, M., Pardowitz, T., Nissen, K., Ulbrich, U., Hundecha, Y., Merz, B., 2014. On the relationship between hydro-meteorological patterns and flood types. J. Hydrol. 519 (Part D), 3249–3262. http://dx.doi.org/10.1016/j.jhydrol.2014.09.089.

Nolin, A.W., Daly, C., 2006. Mapping “at risk” snow in the pacific northwest. J. Hydrometeorol. 7, 1164–1171. http://dx.doi.org/10.1175/JHM543.1.

Parajka, J., Kohnová, S., Bálint, G., Barbuc, M., Borga, M., Claps, P., Cheval, S., Dumitrescu, A., Gaume, E., Hlavčová, K., et al., 2010. Seasonal characteristics of flood regimes across the Alpine–Carpathian range. J. Hydrol. 394, 78–89. http://dx.doi.org/10.1016/j.jhydrol.2010.05.015.

Pattison, I., Lane, S.N., 2012. The relationship between Lamb weather types and long-term changes in flood frequency, river Eden, UK. Int. J. Climatol. 32, 1971–1989. http://dx.doi.org/10.1002/joc.2415.

Perdigão, R.A.P., Blöschl, G., 2014. Spatiotemporal flood sensitivity to annual precipitation: evidence for landscape-climate coevolution. Water Resour. Res. 50, 5492–5509. http://dx.doi.org/10.1002/2014wr015365.

Press, W.H., Teukolsky, S.A., Vetterling, W.T., Flannery, B.P., 2002. Numerical Recipes in C++: The Art of Scientific Computing 2nd edition. Cambridge University Press, Cambridge, UK; New York.

Prudhomme, C., Genevier, M., 2011. Can atmospheric circulation be linked to flooding in Europe? Hydrol. Process. 25, 1180–1190. http://dx.doi.org/10.1002/hyp.7879.

Raff, D.A., Pruitt, T., Brekke, L.D., 2009. A framework for assessing flood frequency based on climate projection information. Hydrol. Earth Syst. Sci. 13, 2119–2136. http://dx.doi.org/10.5194/hess-13-2119-2009.

Ramesh, A., 2013. Response of Flood Events to Land Use and Climate Change. University of Vienna, Austria, (Springer Theses Series).

Remaître, A., Malet, J.-P., Maquaire, O., 2011. Geomorphology and kinematics of debris flows with high entrainment rates: a case study in the South French Alps. Comptes Rendus Geosci. 343, 777–794. http://dx.doi.org/10.1016/j.crte.2011.09.007.

Rousseeuw, P.J., 1987. Silhouettes: a graphical aid to the interpretation and validation of cluster analysis. J. Comput. Appl. Math. 20, 53–65. http://dx.doi.org/10.1016/0377-0427(87)90125-7.

Rousselot, M., Durand, Y., Giraud, G., Mérindol, L., Dombrowski-Etchevers, I., Déqué, M., Castebrunet, H., 2012. Statistical adaptation of ALADIN RCM outputs over the French Alps: application to future climate and snow cover. cryosphere 6, 785–805.

Saez, J.L., Corona, C., Stoffel, M., Berger, F., 2013. Climate change increases frequency of shallow spring landslides in the French Alps. Geology 41, 619–622. http://dx.doi.org/10.1130/g34098.1.

Seibert, J., Vis, M.J.P., 2012. Teaching hydrological modeling with a user-friendly catchment-runoff-model software package. Hydrol. Earth Syst. Sci. 16, 3315–3325. http://dx.doi.org/10.5194/hess-16-3315-2012.

Stanzel, P., Kahl, B., Haberl, U., Herrnegger, M., Nachtnebel, H.P., 2008. Continuous hydrological modelling in the context of real time flood forecasting in alpine Danube tributary catchments. IOP Conf. Ser. Earth Environ. Sci. 4, 012005. http://dx.doi.org/10.1088/1755-1307/4/1/012005.

Steele-Dunne, S., Lynch, P., McGrath, R., Semmler, T., Wang, S., Hanafin, J., Nolan, P., 2008. The impacts of climate change on hydrology in Ireland. J. Hydrol. 356, 28–45.

Steinschneider, S., Brown, C., 2013. A semiparametric multivariate, multisite weather generator with low-frequency variability for use in climate risk assessments. Water Resour. Res. 49, 7205–7220. http://dx.doi.org/10.1002/wrcr.20528.

Tao, F., Zhang, Z., 2011. Impacts of climate change as a function of global mean temperature: maize productivity and water use in China. Clim. Change 105, 409–432. http://dx.doi.org/10.1007/s10584-010-9883-9.

Themeßl, M., Gobiet, A., Heinrich, G., 2012. Empirical-statistical downscaling and error correction of regional climate models and its impact on the climate change signal. Clim. Change 112, 449–468. http://dx.doi.org/10.1007/s10584-011-0224-4.

Thornthwaite, C.W., 1948. An approach toward a rational classification of climate. Geogr. Rev., 55–94. http://dx.doi.org/10.2307/210739.

Timalsina, N.P., Alfredsen, K.T., Killingtveit, Å., 2015. Impact of climate change on ice regime in a river regulated for hydropower. Can. J. Civ. Eng. 42, 634–644. http://dx.doi.org/10.1139/cjce-2014-0261.

Ulbrich, U., Brücher, T., Fink, A.H., Leckebusch, G.C., Krüger, A., Pinto, J.G., 2003. The central European floods of August 2002: part 1 – Rainfall periods and flood development. Weather 58, 371–377. http://dx.doi.org/10.1256/wea.61.03a.

Vaze, J., Post, D.A., Chiew, F.H.S., Perraud, J.M., Viney, N.R., Teng, J., 2010. Climate non-stationarity – Validity of calibrated rainfall–runoff models for use in climate change studies. J. Hydrol. 394, 447–457. http://dx.doi.org/10.1016/j.jhydrol.2010.09.018.

Viglione, A., Chirico, G.B., Komma, J., Woods, R., Borga, M., Blöschl, G., 2010. Quantifying space-time dynamics of flood event types. J. Hydrol. 394, 213–229. http://dx.doi.org/10.1016/j.jhydrol.2010.05.041.

Vormoor, K., Lawrence, D., Heistermann, M., Bronstert, A., 2015. Climate change impacts on the seasonality and generation processes of floods – projections and uncertainties for catchments with mixed snowmelt/rainfall regimes. Hydrol. Earth Syst. Sci. 19, 913–931. http://dx.doi.org/10.5194/hess-19-913-2015.

Wood, A.W., Leung, L.R., Sridhar, V., Lettenmaier, D.P., 2004. Hydrologic implications of dynamical and statistical approaches to downscaling climate model outputs. Clim. Change 62, 189–216. http://dx.doi.org/10.1023/b:clim.0000013685.99609.9e.